Fast estimation of CRS parameters using local slopes

L.T. Santos*, J. Schleicher*, J.C. Costa†, and A. Novais*.

*Dept. of Applied Math., IMECC-UNICAMP, CP 6065, 13083-859 Campinas (SP), Brazil

†Geophysical Institute, University of Pará, 66.075-110, Belém (PA), Brazil

This paper was prepared for presentation at the 11th International Congress of The Brazilian Geophysical Society held in Salvador, Brazil, August 24-28, 2009.

Abstract

The complete set of CRS parameters can be extracted from seismic data by an application of modern local-slope-extraction techniques. The necessary information about the CRS parameters is contained in the slopes of the common-midpoint and common-offset sections at the central point. As demonstrated by a synthetic data example, the slope extraction is sufficiently robust to allow for derivation of the extracted slope field. This enables the calculation of the CRS parameters from the extracted slopes and their derivatives. In this way, the CRS parameter extraction can be sped up by several orders of magnitude.

Introduction

Present-day techniques to estimate the traveltime parameters of the common-reflection-surface (CRS) stack rely on local coherence analyses that are tedious and time-consuming processes (see, e.g., Jäger et al., 2001; Hertweck et al., 2007). However, the extraction of traveltime attributes, particularly local slopes, has received strong attention in the recent past, because local slopes directly extracted from prestack data are useful in a variety of seismic imaging processes. Perhaps, the most visible ones are those connected with seismic tomography, in which not only traveltimes but also slownesses of events and possible other time-domain attributes are used to build a velocity model. Most prominent examples are slope tomography (Sword, 1987; Biondi, 1990), stereotomography (Billette and Lambaré, 1998; Billette et al., 2003) and normal-incidence-point (NIP) wave tomography (Duveneck, 2004).

Recently, Fomel (2002) presented fast techniques how to extract local slopes and even curvature related traveltime parameters. In this paper, we show how the CRS parameters relate to local slopes in order to speed up their extraction. Of course, this relationship is most straightforward for the emergence angle of the normal ray, β, since this parameter is nothing else but a local slope.

The conventional procedure to extract this slope parameter relies on local slant stacks (Ottolini, 1983a). In this method, a local coherence analysis is carried out at each point in the seismic section along short straight-line elements in all possible directions. The direction with the highest coherence defines the slope value at that point.

However, the local-slant-stack approach to local-slope extraction has a number of drawbacks. First of all, the method has a high computational cost. Since the space of local slopes must be closely sampled, there is a high number of coherence analyses to be carried out. The second drawback lies in the method's sensitivity to the aperture of the local slant stacks. An adequate aperture is problem dependent and thus hard to know in advance. Finally, as demonstrated by Schleicher et al. (2009), the extracted slopes are not always reliable, but can be biased towards too high dips.

For this reason, Schleicher et al. (2009) studied alternative, faster and more reliable ways to extract local slopes. They showed that using modern extraction techniques, local slopes can be extracted faster and more reliably than using local slant-stacks. Therefore, the question arises whether these kind of techniques can be extended to allow for the extraction of the remaining CRS parameters.

In this work, we demonstrate that such an extension is possible. We show how the complete set of CRS parameters can be estimated by the application of modern, more advanced local-slope-extraction techniques, that are several orders of magnitude faster than conventional local coherence analysis.

Hyperbolic Moveouts

Let us now study how the local slopes can be used to extract information about the CRS parameters. To understand the relationship between local slopes and the CRS parameters, let us start with a brief review of the underlying traveltime approximations.

Common-reflection-surface traveltime

The common reflection surface (CRS) method, introduced by Peter Hubral and co-workers (see, e.g., Hubral et al., 1998) represents a natural extension of the CMP method in two important aspects. Firstly, for each stacking trace location (above referred to as the central point of the CMP gather, now called simply the central point), the CRS method considers a supergather of source-receiver pairs, arbitrarily located with respect to the central point. In other words, the gather is not restricted to the CMP condition. Secondly, not only the NMO velocity, but also other additional parameters describe the traveltime function and can thus be extracted from the data. In the 2D situation, studied in this work, three parameters are determined for each central point and all ZO traveltime samples. The procedure is performed automatically, with no *a priori* selection of traveltime samples.

To be able to stack source-receiver pairs that do not conform to the CMP condition, the CRS method utilizes the (generalized) hyperbolic moveout,

$$t_{CRS}(x,h) = \sqrt{[t_0 + A\,(x-x_0)]^2 + B\,(x-x_0)^2 + C\,h^2}, \quad (1)$$

where x and h denote the midpoint and half-offset coordinates of the source and receiver pair, x_0 is the midpoint coordinate of the central point, and $t_0 = t_{CRS}(x_0, 0)$ is the ZO traveltime at the central point. As shown in Hubral et al. (1998), the parameters A, B and C are related to the more physical CRS parameters β, K_N and K_{NIP}, by the relationships

$$A = \frac{2\sin\beta}{v_0}, \quad B = \frac{2t_0\cos^2\beta}{v_0}K_N,$$
$$\text{and} \quad C = \frac{2t_0\cos^2\beta}{v_0}K_{NIP} = \frac{4}{V^2}, \quad (2)$$

where v_0 denotes the near-surface medium velocity at the central point and where V represents the stacking or NMO velocity.

Observe that formula (1) reduces to the normal-moveout equation (see below) for source-receiver pairs in the central CMP gather, i.e., for $x = x_0$. Another important observation is that parameters A, B, and C depend on t_0. Finally, note that the original CRS parameters β, K_N, and K_{NIP} can be calculated once all three parameters A, B, and C are known.

Common-midpoint traveltime

In the 2D situation of a single (horizontal) seismic line and within a given common midpoint (CMP) gather at a fixed central point x_0, the traveltime can be approximated by the *Normal Moveout (NMO)* function,

$$t_{CMP}(h) = \sqrt{t_0^2 + C\,h^2}. \quad (3)$$

Here, t_{CMP} is the reflection traveltime, h is the half-offset, and $t_0 = t_{CMP}(0)$ is the CMP zero-offset (ZO) traveltime at the central point of the CMP gather.

However, this parameter C is directly related to the ray parameter for the reflection ray in the CMP gather, i.e., the traveltime slope of equation (3) (see, e.g., Castagna and Backus, 1993). The derivative of equation (3) with respect to source-receiver offset $2h$ yields

$$p = \frac{1}{2}\frac{d}{dh}t_{CMP} = \frac{C\,h}{2\,t_{CMP}}. \quad (4)$$

Thus, if we know the local slope $p = p(h, t_{CMP})$ at a point (h, t_{CMP}) in a CMP gather, we can use equations (3) and (4) to eliminate C from the moveout equation. This yields the NMO coordinate map

$$t_0 = \sqrt{t_{CMP}^2 - 2\,h\,t_{CMP}\,p(h,t_{CMP})}, \quad (5)$$

which describes the relationship between the time coordinates t_{CMP} in a CMP section and t_0 of a ZO trace at x_0. Equation (5) can be immediately used for an automatic NMO correction (Ottolini, 1983b), since it tells us how to move a pixel of information from coordinates (h, t_{CMP}) in the CMP section to (h, t_0) in the NMO corrected section.

On the other hand, equation (4) provides us with the first relationship between a curvature parameter and a local slope. Rewriting equation (4), we see that parameter C at half-offset h and ZO time t_0 is given by

$$C(h, t_0) = 2\,t_{CMP}\,p(h, t_{CMP})\,/\,h. \quad (6)$$

Equations (5) and (6) describe the procedure that achieves the construction of a C-parameter section. Each extracted local slope p at a position (h, t) in the CMP section is corrected with the factor $2t/h$ and the result is transferred automatically to the C-parameter section at (x_0, t_0). The final $C(x_0, t_0)$ is calculated by averaging at x_0 over all $C(x_0, t_0)$ from all half-offsets.

Common-offset traveltime

The remaining two CRS parameters, A and B can be determined from a common-offset (CO) gather in the vicinity of x_0. For the case of a CO gather with a fixed $h > 0$, formula (1) reduces to

$$t_{CO}(x) = \sqrt{t_{CMP}(h)^2 + 2\,A\,t_0\,(x-x_0) + D\,(x-x_0)^2}, \quad (7)$$

where $D = A^2 + B$ and t_{CMP} is the traveltime for the offset ray with midpoint at x_0. It is given in terms of the ZO traveltime by equation (3).

A similar scheme to equations (5) and (6) can be applied to extract the remaining CRS parameters from a CO gather with fixed $h > 0$ in the vicinity of the central point x_0. From traveltime formula (7), we obtain the local slope q at a point (x, t_{CO}) in the CO gather as

$$q = \frac{d}{dx}t_{CO} = \frac{A\,t_0 + D\,(x-x_0)}{t_{CO}}. \quad (8)$$

Taking the derivative of equation (8) with respect to x, and recombining the resulting equation for $q_x = dq/dx$ with equation (8), we arrive at

$$D(x, t_{CO}) = q(x, t_{CO})^2 + t_{CO}\,q_x(x, t_{CO}). \quad (9)$$

Equation (9) tells us how to determine the value of the combined parameter D of equation (7) at a certain point (x, t_{CO}) in the CO section. However, this value of D is still associated with a point (x, t_{CO}) in the CO section and needs to be attributed to its respective coordinate t_0 in the ZO section to be constructed. For this purpose we solve equation (8) for A and substitute the resulting expression in equation (7). Solving for the CMP traveltime, we obtain the coordinate map

$$t_{CMP} = \sqrt{t_{CO}^2 - 2\,q(x,t_{CO})\,t_{CO}\,(x-x_0) + D\,(x-x_0)^2}, \quad (10)$$

between the CO and CMP sections. Map (10) can be executed once q and q_x have been detected at every point (x, t_{CO}) in the CO section. Finally, the time coordinate t_{CMP} is related to its associated ZO traveltime t_0 through formula (5).

Combining the above equations and coordinate maps, we can construct the sections for the parameters A and B at

time t_0. Parameters A and B are thus given by the following pair of equations:

$$A(x_0,t_0) = \frac{q(x,t_{CO})\,t_{CO} - D(x,t_{CO})\,(x-x_0)}{t_0}, \quad (11)$$

$$B(x_0,t_0) = D(x_0,t_0) - A(x_0,t_0)^2. \quad (12)$$

This mapping procedure can be applied for different CO sections around the central point x_0. As in the parameter C case, the values of A and B are transfered to the respective parameter sections at (x_0,t_0). The final values of A and B are obtained by averaging over all values that are attributed to the same point (x_0,t_0).

Extracting the local slopes

The extraction of local slopes is done by so-called plane-wave destructors. The differential equation that describes a local plane-wave event in a seismic section is given by (Claerbout, 2004)

$$\psi_y(y,t) + s\,\psi_t(y,t) = 0, \quad (13)$$

where $\psi(y,t)$ is the wavefield, t is the time coordinate, and y is the horizontal coordinate, i.e., offset ($2h$) in the case of a CMP section or midpoint (x) in the case of a CO section. Quantity s represents the local slope (i.e., p or q in a CMP or CO section), which may depend on y and even on t, i.e., generally, $s = s(y,t)$.

To extract the slopes, we use basically the technique presented in Claerbout (2004) and Schleicher et al. (2009). We just employ a few small alterations in the implementation that we found to turn the process more stable.

For each pair (ξ,τ) in the seismic section, we select a small window of points y_i, t_j with $(i,j) \in W$. Let $\Psi_y(y_i,t_j)/\Delta y$ and $\Psi_t(y_i,t_j)/\Delta t$ be the discretized values for the derivatives ψ_y and ψ_t, respectively, in the selected window, with Δy and Δt being the respective sample sizes. In order to accomplish with equation (13), we minimize the quadratic residual

$$R(s) = \sum_{(i,j)\in W} \left[\Psi_y(y_i,t_j) + s\frac{\Delta y}{\Delta t}\,\Psi_t(y_i,t_j)\right]^2. \quad (14)$$

The solution is easily found as

$$s^* = s^*(\xi,\tau) = -\frac{\Delta t}{\Delta y}\,\frac{\sum_{(i,j)\in W}\Psi_y(y_i,t_j)\Psi_t(y_i,t_j)}{\sum_{(i,j)\in W}\Psi_t^2(y_i,t_j)}, \quad (15)$$

where (ξ,τ) is the center of the selected window. One measure for the fit is given by the normalized residual. To avoid the problems reported in Schleicher et al. (2009) at local slopes close to zero, we use the slightly modified coherence measure

$$E(\xi,\tau) = 1 - \frac{R(s^*)}{\sum_{(i,j)\in W}\left[\Psi_y^2(y_i,t_j) + \Psi_t^2(y_i,t_j)\right]}. \quad (16)$$

Synthetic Examples

For the numerical experiments we used a simple synthetic model of a stratified medium with homogeneous layers as shown in Figure 1, with a fixed central point at $x_0 = 5$ km. We simulated a CMP section with 70 half-offsets ranging from -1 km to 1 km, and a single CO section with constant half-offset of 250 m and 51 midpoints ranging from 4.5 km to 5.5 km. In both simulations the time sample was 4 ms. For better control over the CRS parameters, we simulated all reflection events as if the velocities in the model where constant rms velocities down to the corresponding reflector. The rms velocity for the shallowest reflector was 4.0 km/s, increasing by 0.2 km/s for each layer to 5.0 km/s for the deepest one. Also shown in Figure 1 is the point x_0 for which we carry out the analysis.

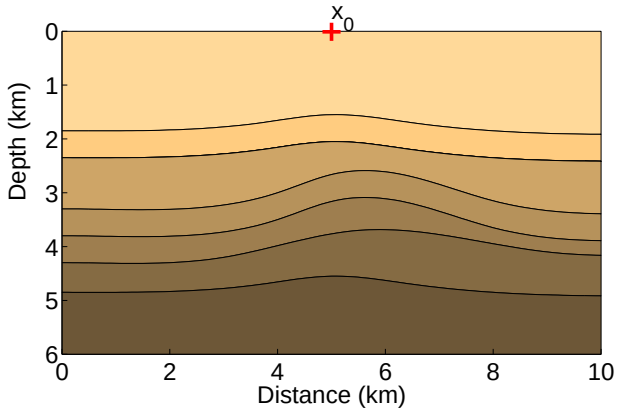

Figure 1: Synthetic model for the experiments

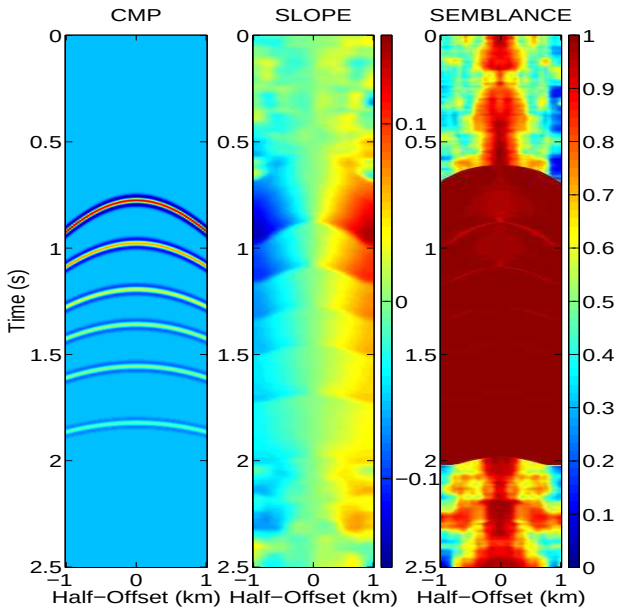

Figure 2: Experiment without noise: CMP, slope and semblance sections

Since real data consist of many CO gathers for different offsets, these even could be used to improve redundancy. However, since the traveltime approximations are valid in the vicinity of the normal ray, too far offsets should be avoided. In our numerical experiments, best results were achieved by using only one or two small offsets.

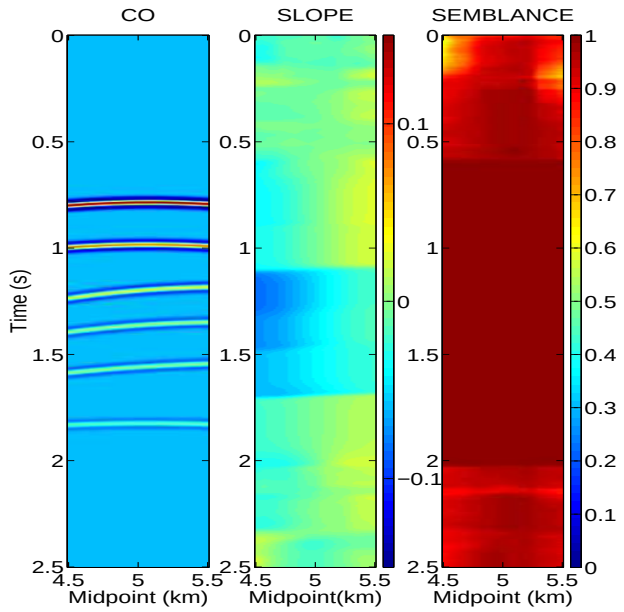

Figure 3: Experiment without noise: CO, slope and semblance sections

Noise-free data

The results of the CRS parameter extraction for noise-free data are shown in Figures 2 to 4. In Figure 2 we see the CMP section and the corresponding slope (p) and semblance (E) sections as obtained using equations (15) and (16). The extraction window used 21 traces and 41 time samples. The extracted slopes values correspond very well to the expected values. The semblance is very high in the time interval of the events, indicating high reliability of the extracted slope values.

Figure 3 depicts the corresponding CO section together with its extracted slope (q) and semblance sections. Again, the extracted slope values correspond perfectly to the dips in the CO section, and the high semblance in the time interval of the events indicates high reliability.

The values of the CRS parameters A, B and C at the chosen point x_0 (only one trace) were then determined from these extracted slopes using equations (6), (11) and (12). The results are depicted in Figure 4 (red lines), together with the respective exact values (blue crosses). Of course, true values are only available at the reflection events while the extraction procedure yields values at all times. Figure 4 also shows the values of the accumulated semblances (S) for p and q. These are the mean values of the semblances of all values of the parameters A, B and C that contributed to the final values. As usual for noise-free data, the semblance is very high everywhere.

The overall quality of the so extracted CRS parameters is more than satisfying. Parameters C and A (related to K_{NIP} and β) have been determined near perfectly. Parameter B (related to K_N), known to be the most unstable parameter, has not been recovered with the same precision. However, the extracted values show the general trend and only slightly underestimate the true values.

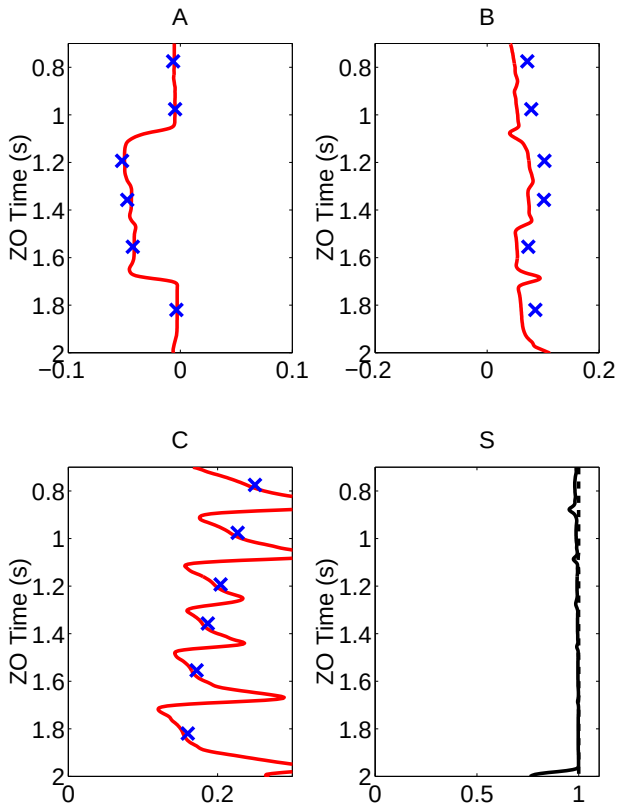

Figure 4: Experiment without noise: CRS parameters (A, B, C) and semblances (S). The exact are the blue crosses and the estimated ones are the red lines.

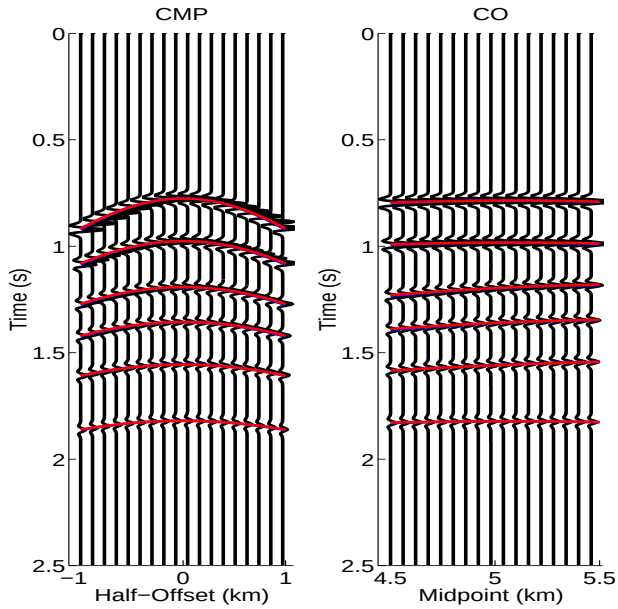

Figure 5: Experiment without noise: CMP and CO sections with exact (blue) and estimated (red) traveltimes.

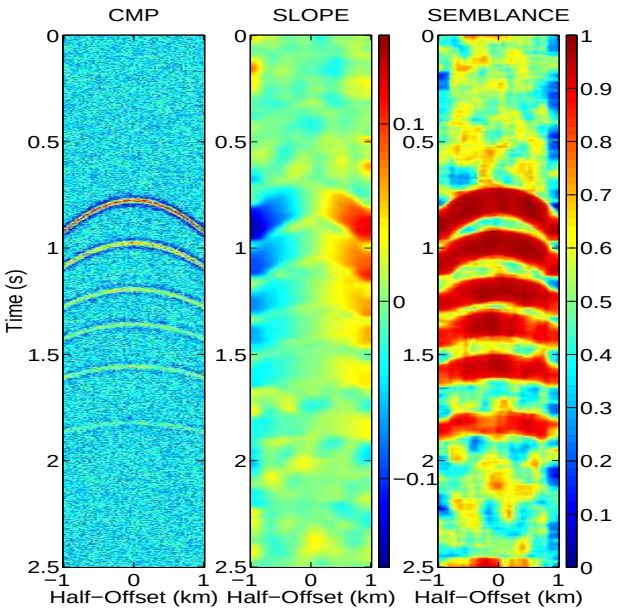

Figure 6: Experiment with 30% added noise: CMP, slope and semblance sections.

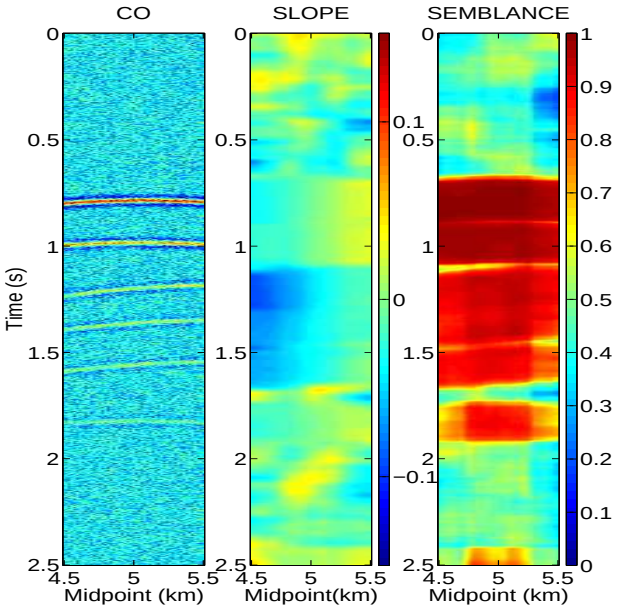

Figure 7: Experiment with 30% added noise: CO, slope and semblance sections.

Another way of evaluating the quality of the extracted CRS parameters is by seeing how well the corresponding traveltime approximations fit the data Figure 5 shows this analysis. We see that the CMP and CO reflection events are perfectly fitted by traveltimes (3) and (7) using the extracted parameters (red lines), confirming their high quality. The blue lines representing the traveltime curves with the exact parameter values are invisible because they are entirely covered by the red lines.

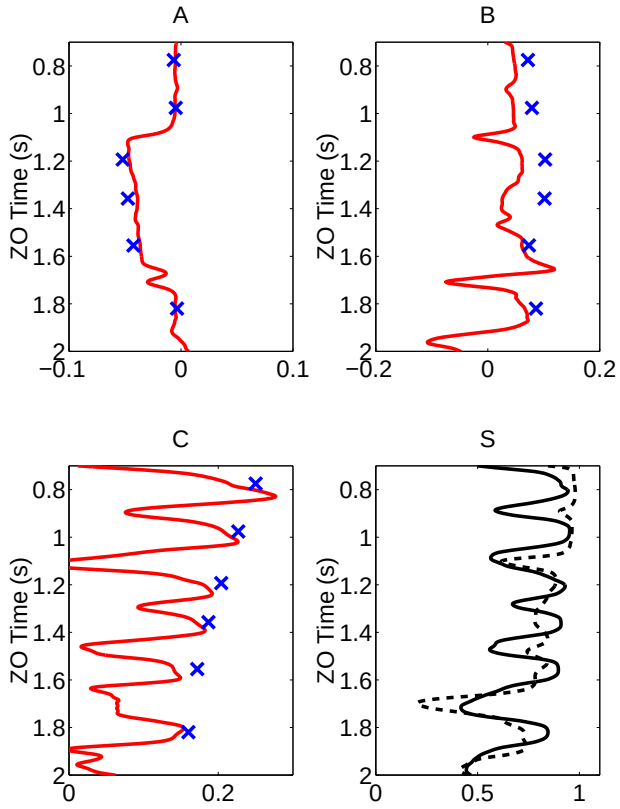

Figure 8: Experiment with 30% added noise: CRS parameters (A, B, C) and semblances (S). The exact are the blue crosses and the estimated ones are the red lines.

Noisy data

For a more realistic test of the proposed extraction method, it is important to investigate how it reacts to the presence of noise. Therefore, we have repeated the above experiment after 30% adding random noise to the synthetic data. In other words, the noise level was chosen such that the signal-to-noise ratio for the strongest arrival, the reflection from the topmost reflector, was about 3. This resulted in a signal-to-noise for the weakest arrival, the reflection from the deepest reflector, of about 1. Figures 6 to 8 show the extraction results for the noisy data. The general behavior of the slope and semblance sections of the CMP and CO gathers (Figures 6 and 7) is very similar to the corresponding sections for the noise-free situation (Figures 2 and 3), demonstrating that the estimation of local slopes is sufficiently stable at this noise level.

Figure 8 compares the extracted parameter values (red lines) to the exact ones (blue crosses). The results are still satisfactory. Parameters A and C have lost almost no quality in comparison to the noise-free situation (Figure 4). The noise seems to influence mainly the extracted values of parameter B, the quality of which has further deteriorated. It is to be noted that for the noisy data, the accumulated semblance S exhibits significant peaks at the actual reflection times, thus carrying useful information on where the extracted parameter values are actually reliable.

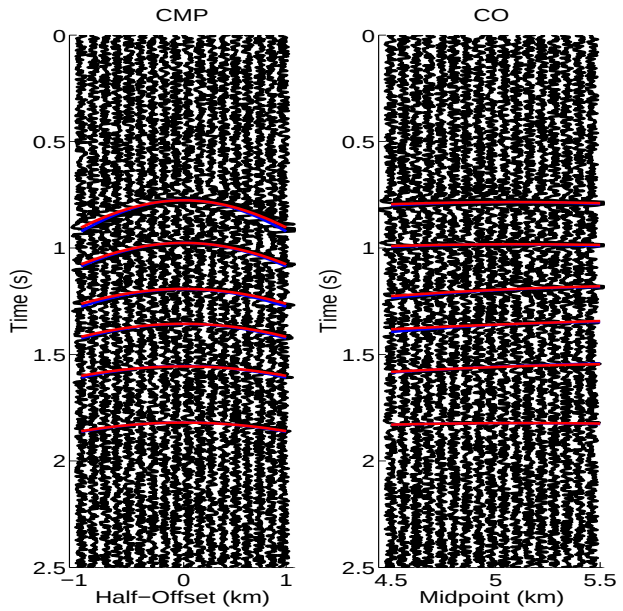

Figure 9: Experiment with 30% added noise: CMP and CO sections with exact (blue) and estimated (red) traveltimes.

The fit achieved with these extracted parameters is evaluated in Figure 9. We see that the small errors in parameter C already lead to small deviations between the exact and fitted traveltime curves (blue and red lines, respectively) in the CMP gather. On the other hand, the larger errors in B lead to almost no deviation between the exact and fitted traveltime curves in the CO gather. This behavior is the reason why it is almost impossible by any method to extract reliable values for B.

These numerical experiments demonstrate that the estimation of CRS parameters from local slopes is sufficiently stable to permit their automatic extraction, even for noisy data. We stress again that this extraction procedure is orders of magnitude faster than the conventional method by local coherence analyses.

Conclusions

CRS parameter extraction by local coherence analysis has a number of drawbacks. First and most important of all, the method has a high computational cost. Since the space of possible parameter values must be closely sampled, there is a high number of coherence analyses to be carried out. The second drawback lies in the method's sensitivity to the aperture of the local stacking operators. An adequate aperture is problem dependent and thus hard to know in advance.

In this work, we have shown that it is possible to overcome these problems by a different approach to parameter extraction. We have presented an application of modern local-slope-extraction techniques so as to allow for the detection of the complete set of CRS parameters. The necessary information about the CRS parameters is contained in the slopes of the common-midpoint and common-offset sections at the central point. As demonstrated by a synthetic data example, the slope extraction is sufficiently robust to allow for derivation of the extracted slope field. This enables the calculation of the CRS parameters from the extracted slopes and their derivatives. In this way, the CRS parameter extraction can be sped up by several orders of magnitude.

Acknowledgments

We thank the Brazilian research agencies, CAPES, CNPq and FAPESP, as well as Petrobras and the sponsors of the Wave Inversion Technology (WIT) consortium for their support.

References

Billette, F. and G. Lambaré, 1998, Velocity macro-model estimation from seismic reflection data by stereotomography: Geophys. J. Int., **135**, 671–690.

Billette, F., S. Le Bégat, P. Podvin, and L. G., 2003, Pratical aspects and applications of 2D stereotomography: Geophysics, **68**, 1008–1021.

Biondi, B., 1990, Seismic velocity estimation by beam stack: PhD thesis, Stanford University.

Castagna, J. P. and M. M. Backus, 1993, Offset-dependent reflectivity – theory and practice of avo analysis: SEG.

Claerbout, J. F., 2004, Earth sounding analysis: Processing versus inversion: Blackwell Scientific Publications.

Duveneck, E., 2004, 3D tomographic velocity model estimation with kinematic wavefield attributes: Geophysical Prospecting, **52**, 535–545.

Fomel, S., 2002, Applications of plane-wave destruction filters: Geophysics, **67**, 1946–1960.

Hertweck, T., J. Schleicher, and J. Mann, 2007, Data stacking beyond CMP: The Leading Edge, **26**, 818–827.

Hubral, P., G. Höcht, and R. Jäger, 1998, An introduction to the common reflection surface stack: 60th EAGE Conference & Exhibition, Expanded Abstracts, **Session**, 01–19.

Jäger, R., J. Mann, G. Höcht, and P. Hubral, 2001, Common-reflection-surface stack: Image and attributes: Geophysics, **66**, 97–109.

Ottolini, R., 1983a, Signal/noise separation in dip space: SEP report, **SEP-37**, 143–149.

———, 1983b, Velocity independent seismic imaging: SEP report, **SEP-37**, 59–67.

Schleicher, J., J. C. Costa, L. T. Santos, A. Novais, and M. Tygel, 2009, On the estimation of local slopes: Geophysics, **74**. In print.

Sword, C. H., 1987, Tomographic determination of interval velocities from reflection seismic data: The method of controlled directional reception: PhD thesis, Stanford University.